https://doi.org/10.1016/j.ijleo.2020.164984

An intelligent joint filter for vector tracking loop considering noise interference

Jie Dou [1], Bing Xu [2] and Lei Dou [1,*]

[1] School of National Key Laboratory of Transient Physics, Nanjing University of Science and Technology, Nanjing 210094, China; doujienjust@163.com (J.D.)

[2] Interdisciplinary Division of Aeronautical and Aviation Engineering, The Hong Kong Polytechnic University, Kowloon, Hong Kong, China; pbing.xu@polyu.edu.hk (B.X.)

* Correspondence: douleijs@163.com

Received: date; Accepted: date; Published: date

Abstract: In this paper, we propose an intelligent joint filter (JF) for enhancing the performance of vector tracking loop (VTL) in the Global Navigation Satellite System (GNSS). The JF combines the advantages of extended Kalman filter (EKF) and unbiased finite-impulse response (UFIR) filter. To this end, a supervised machine learning algorithm, named Gaussian mixture model (GMM) clustering, was used for providing excellent joint strategy. Those three types of filter-based vector tracking loop were first implemented and then processed with a set of raw satellite signals based on the software-defined receiver (SDR). Finally, comparative analyses and results of the tracking performance of EKF/UFIR/JF were carried out. Results show that the EKF-VTL has optimal tracking performance but sensitive to the noise statistics, which means it's not robust. The UFIR-VTL is suboptimal but more robust compare to EKF-VTL. The proposed JF-VTL is both optimal and robust.

Keywords: Global Navigation Satellite System (GNSS); vector tracking loop (VTL); extended Kalman filter (EKF); unbiased finite-impulse response (UFIR) filter; Gaussian mixture model (GMM) clustering; joint filter (JF)

---

1. Introduction

In response to the increasingly severe Global Navigation Satellite System (GNSS) environment, many techniques have been widely developed and applied in GNSS, such as antenna design, algorithm improvement and external aids [1–4]. Among these techniques, the vector tracking loop (VTL) technique has been extensively exploited in the GNSS receiver, because it is low cost and easy to implement [5]. The advantages of VTL over the conventional scalar tracking loop (STL) have been proved in many tough scenarios, e.g., high dynamics, intermittent signal outages, multipath interference and non-line-of-sight reception [6–8].

In VTL, all the tracking information of working channels is deeply coupled and interacted with each other. That is, the VTL is supervised because it combines all the tracking channels and takes full advantage of the relativity between them via a single integration filter, which is typically based on the extended Kalman filter (EKF). However, according to the Kalman filter theory, the optimal estimation of EKF depends on the exactly known noise statistics, which refer to the process noise covariance matrix $\boldsymbol{Q}$ and the measurement noise covariance matrix $\boldsymbol{R}$. Otherwise, the filter results are inaccurate or even diverging [9]. Aim to this weakness, some scholars propose to use adaptive algorithms to adjust the noise online, it works but it degrades the real-time performance and does not lead to satisfactory results for time-varying systems in most cases [10,11]. Besides, the $\boldsymbol{R}$ update time and window size N of adaptive EKF are still determined empirically [12].

In recent years, another popular Kalman-like filter, namely unbiased finite-impulse response (UFIR) filter, attracted the numerous attention of scholars. The UFIR filter was first proposed by Yuriy S. Shmaliy [13] and has been successfully applied to the discrete time-varying nonlinear systems [14,15]. Unlike EKF, the UFIR filter can ignore noise statistics completely, which means that it is immune to the errors in the noise statistics. Another advantage of UFIR over the EKF algorithm is that it only requires an optimal horizon of N_{opt} points for minimizing the mean-square error (MSE). Fortunately, the N_{opt}

can be accurately achieved via measurements [16], which is much easier than for the noise statistics required by the EKF.

Because of above mentioned, the purpose of this letter is to enhance the tracking performance of VTL in terms of both accuracy and robustness. To achieve this, firstly, a set of raw satellite data was collected from the open area by a vehicle motion experiment. Secondly, the EKF and UFIR algorithm was used to build the VTL, respectively, and were processed the data through the same software-defined receiver (SDR). Based on this, tracking measurements like code frequency, pseudorange will be extracted, and the performance comparative analysis of these two methods is carried out. Finally, we unite the EKF and UFIR to propose a joint filter (JF), in which the Gaussian mixture model (GMM) clustering algorithm was used to provide a better joint strategy. As a surprised Machine learning theory, GMM clustering is a distribution-based algorithm. In GMM, the probability density distribution of samples can be determined by the weighted sum of several Gaussian distribution functions [17,18]. Compared with the existing works, the main contributions of this letter could be summarized as follows:

(1) We use UFIR algorithm to construct the VTL and verify its feasibility, which demonstrated suboptimal but robust compare to EKF-VTL.

(2) Based on the first contribution, we further combine the advantages of EKF and the UFIR algorithm to build the joint filter (JF), which can achieve better tracking performance under different noise conditions.

The rest of the paper is organized as follows. Section 2 introduces the methodology of the conventional VTL, which is based on the EKF algorithm and the proposed UFIR-VTL. The principles and implementation details of the proposed fusion algorithm are presented in Section 3. Experiment results to verify the tracking performance of the proposed method and some comparative analysis are provided in Section 4 and the conclusions of the study are presented in Section 5.

2. Methodology

2.1. VTL model

As mentioned earlier, by making the most of the internal connections between the tracking channels, VTL couples all the channels information together using a single navigation processor. As shown in Fig. 1, based on the navigation solutions and the satellite ephemeris, the navigation processor can predict the receiver states information including position, velocity, clock bias and drift. In specific, the code phase errors and the frequency errors obtained from the discriminator output are not used to correct the corresponding numerically controlled oscillator (NCO) directly. The discriminator outputs are converted to pseudo-range error and pseudo-range rate error measurements. With the navigation solution and satellite ephemeris, the code and frequency errors at the next epoch can be predicted to drive the NCO. If only use the pseudoranges information in the state formulation of EKF, the vectorized method is called VDLL. Furthermore, both pseudoranges and pseudoranges rates can be used to establish VDFLL. In this letter, VDLL is the objective.

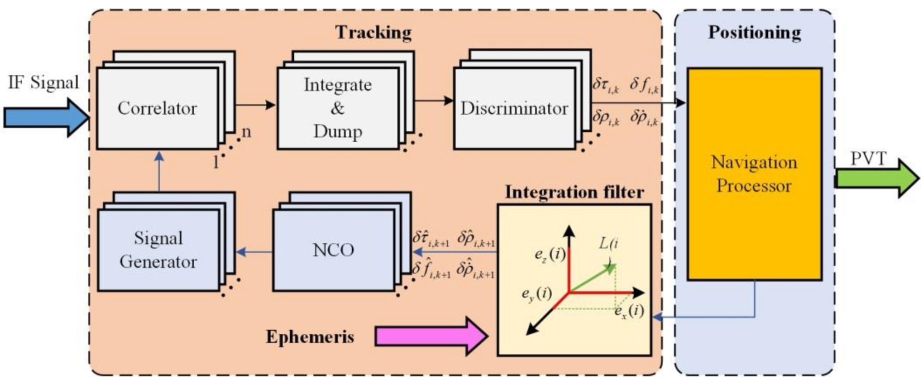

Fig. 1. Block diagram of VTL.

In VTL, the system equation at epoch k is as follows:

$$\hat{\boldsymbol{X}}_k = \boldsymbol{\Phi}_{k-1}\hat{\boldsymbol{X}}_{k-1} \tag{1}$$

where $\boldsymbol{X} = \begin{bmatrix} \delta p_x & \delta p_y & \delta p_z & \delta t \end{bmatrix}^T$, is the state vector, in which δp_x δp_y, and δp_z are the three-dimensional receiver position errors in an earth-centered and earth-fixed (ECEF) coordinates; δt is the receiver clock bias error.; $\boldsymbol{\Phi}_{k-1} = \boldsymbol{I}_{4\times4}$. The symbol "$\wedge$" denotes the estimates.

The measurement equation is the function of the state vector with a first-order Taylor's expression, which is given by:

$$\boldsymbol{Z}_k = \boldsymbol{H}_k \hat{\boldsymbol{X}}_k \tag{2}$$

where $\boldsymbol{Z} = \begin{bmatrix} \delta\rho_1 & \delta\rho_2 & \cdots & \delta\rho_{\mathrm{n}} \end{bmatrix}$, is the measurement vector; $\delta\rho$ represents the pseudorange error; n is the number of satellites involved in tracking; $\boldsymbol{H}$ is the measurement matrix, calculated by:

$$\boldsymbol{H} = \begin{bmatrix} e_{1,x} & e_{1,y} & e_{1,z} & 1 \\ e_{2,x} & e_{2,y} & e_{2,z} & 1 \\ \vdots & \vdots & \vdots & \vdots \\ e_{n,x} & e_{n,y} & e_{n,z} & 1 \end{bmatrix} \tag{3}$$

where e is the line-of-sight (LOS) vector between the receiver and the satellites.

2.2. EKF-based tracking loop

The EKF algorithm for the non-linear system is given as follows:

(1) Time update

$$\hat{\boldsymbol{X}}_{k/k-1} = \boldsymbol{\Phi}_{k/k-1} \hat{\boldsymbol{X}}_{k-1} \tag{4}$$

$$\boldsymbol{P}_{k/k-1} = \boldsymbol{\Phi}_{k/k-1} \boldsymbol{P}_{k/k-1} \boldsymbol{\Phi}_{k/k-1}^{\mathrm{T}} + \boldsymbol{Q}_{k-1} \tag{5}$$

(2) Measurement update

$$\boldsymbol{K}_k = \boldsymbol{P}_{k/k-1}\boldsymbol{H}_k^{\mathrm{T}}(\boldsymbol{H}_k\boldsymbol{P}_{k/k-1}\boldsymbol{H}_k^{\mathrm{T}} + \boldsymbol{R}_k)^{-1} \tag{6}$$

$$\hat{\boldsymbol{X}}_{k/k} = \hat{\boldsymbol{X}}_{k/k-1} + \boldsymbol{K}_k(\boldsymbol{Z}_k - \boldsymbol{H}_k\hat{\boldsymbol{X}}_{k/k-1}) \tag{7}$$

$$\boldsymbol{P}_{k/k} = [\boldsymbol{I} - \boldsymbol{K}_k\boldsymbol{H}_k]\boldsymbol{P}_{k/k-1} \tag{8}$$

Here, $\boldsymbol{K}$ is the Kalman gain and used to correct the measurements; $\hat{\boldsymbol{X}}_{k/k}$ and $\boldsymbol{P}_{k/k}$ are the estimate and error covariance, respectively. It is should be noted that, to make the EKF optimal, the process noise covariance $\boldsymbol{Q}$ and measurement noise covariance $\boldsymbol{R}$ should be known exactly.

2.3. UFIR filter

Different from the EKF, the UFIR operates with only the averaging horizon of N points, instead of the noise statistics. To reduce the computational burden, the iteration of UFIR is used in this letter. As shown in Fig. 2, the UFIR algorithm operates from m to k. The iteration estimates $\hat{\boldsymbol{X}}_s$ at s in a batch form on a horizon $[m,s]$, and then updates estimates iteratively to reach the final value at k.

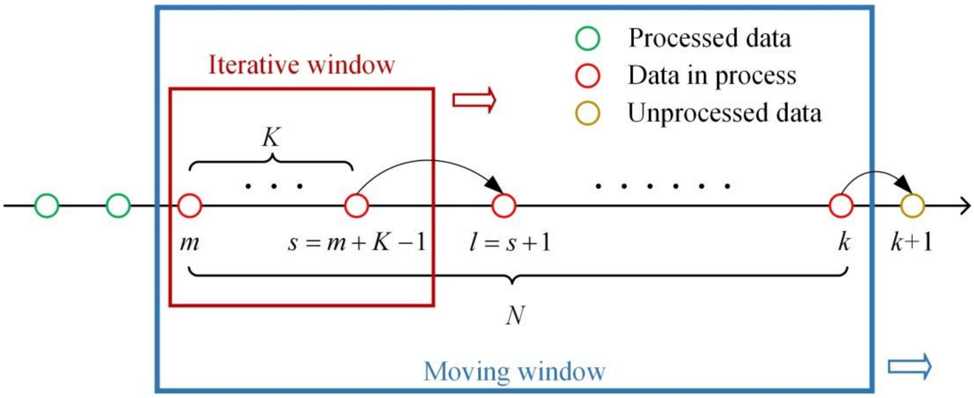

Fig. 2. The flow chart of the iterative UFIR algorithm.

The algorithm can be written as follows:

(1) Preparation

$$\hat{\boldsymbol{X}}_s = \left(\boldsymbol{C}_{m,s}^T \boldsymbol{C}_{m,s}\right)^{-1} \boldsymbol{C}_{m,s}^T \boldsymbol{Z}_{m,s} \tag{9}$$

where $\boldsymbol{C}_{m,s}$ and $\boldsymbol{y}_{m,s}$ are the mapping matrix and extended observation vector, respectively, and represented as:

$$\boldsymbol{Z}_{m,s} = \left[\boldsymbol{Z}_m \quad \boldsymbol{Z}_{m+1} \quad \cdots \quad \boldsymbol{Z}_s\right]^T \tag{10}$$

$$\boldsymbol{C}_{m,s} = \begin{bmatrix} \boldsymbol{H}_m (\mathit{\Gamma}_s^{m+1})^{-1} \\ \boldsymbol{H}_{m+1} (\mathit{\Gamma}_s^{m+2})^{-1} \\ \vdots \\ \boldsymbol{H}_{s-1} \boldsymbol{F}_s^{-1} \\ \boldsymbol{H}_s \end{bmatrix} \tag{11}$$

where $\mathit{\Gamma}_s^m$ is an auxiliary matrix, given by:

$$\mathit{\Gamma}_s^m = \begin{cases} \Phi_s \Phi_{s-1} \cdots \Phi_m, & m \le s \\ \boldsymbol{I}, & m = s+1 \\ 0 & others \end{cases} \tag{12}$$

(2) Time update

$$\hat{\boldsymbol{X}}_{\bar{l}} = \Phi_l \hat{\boldsymbol{X}}_{l-1} \tag{13}$$

(3) Measurement update

$$\boldsymbol{G}_l = [\boldsymbol{H}_l^T \boldsymbol{H}_l + (\Phi_l \boldsymbol{G}_{l-1} \Phi^T)^{-1}]^{-1} \tag{14}$$

$$\boldsymbol{K}_l = \boldsymbol{G}_l \boldsymbol{H}_l^T \tag{15}$$

$$\hat{\boldsymbol{X}}_l = \hat{\boldsymbol{X}}_{\bar{l}} + \boldsymbol{K}_l (\boldsymbol{Z}_l - \boldsymbol{H}_l \hat{\boldsymbol{X}}_{\bar{l}}) \tag{16}$$

where $\boldsymbol{G}_l$ is the generalized noise power gain (GNPG), $\boldsymbol{K}_l$ represents the bias correction gain, not the Kalman gain in Equation (6).

The UFIR filtering algorithm is easy to implement in nonlinear systems as EKF. The only tuning parameter required is the optimal horizon N_{opt}, to minimize the mean-square error (MSE), which can be obtained by minimizing the trace of the error covariance matrix $\boldsymbol{P}_k$, as follows [14]:

$$N_{opt} = \arg\min_N \{\mathrm{tr}\mathbf{P}_k(N)\} \tag{17}$$

where,

$$\mathbf{P}_k(N) = \mathrm{E}\{[\boldsymbol{x}_k - \hat{\boldsymbol{x}}_k(N)][\boldsymbol{x}_k - \hat{\boldsymbol{x}}_k(N)]^T\} \tag{18}$$

3. Proposed method

3.1. Architecture

To combine the advantages of EKF and UFIR, we first run these two algorithms-based VTL simultaneously, to obtain two different estimates $\hat{\boldsymbol{X}}_k^{EKF}$ and $\hat{\boldsymbol{X}}_k^{UFIR}$. Then, we fuse these estimates with proper weights using the GMM clustering strategy. The GMM clustering is used because it can maximize the probability distribution of the samples and output the probability value. The architecture of the proposed method is shown in Fig. 3.

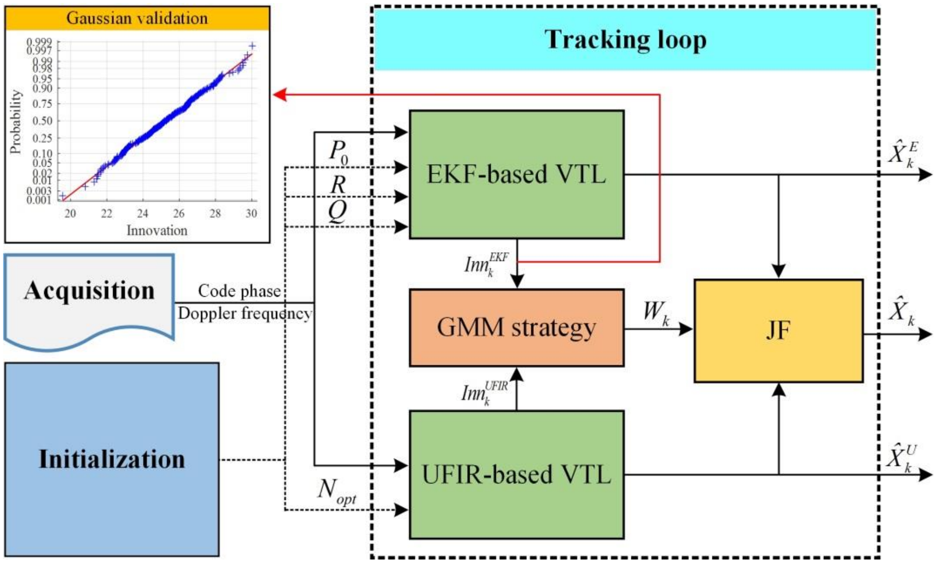

Fig. 3. The architecture of the proposed method. The upper left block diagram exhibits that the samples extracted from the tracking loop follow the Gaussian distribution since the data points ('+') appear along the reference line (red).

3.2. GMM clustering

GMM is defined as the combination of finite Gaussian probability density functions, which represent the distribution of samples and can be expressed as follows [18]:

$$p(x \mid \Phi) = \sum_{l=1}^{M} \omega_l \, p(x \mid \mu_l, \Sigma_l) \tag{19}$$

where x is the sample data; M is the number of Gaussian components; Φ is the model parameters, including mean vector μ, covariance matrix Σ and weight ω, satisfy $\sum_{l=1}^{M} \omega_l = 1$; $p(x \mid \mu_l, \Sigma_l)$ represents the Gaussian component, and can be obtained by:

$$p(x \mid \mu_l, \Sigma_l) = \frac{1}{(2\pi)^{\frac{D}{2}} \left|\Sigma_l\right|^{\frac{1}{2}}} \exp[-\frac{1}{2}(x-\mu_l)^T \Sigma^{-1}(x-\mu_l)] \tag{20}$$

where D is the dimension of x.

To obtain the maximum likelihood of probability density, the expectation-maximization (EM) algorithm is usually used to estimate the GMM parameter. The EM algorithm is as follows:

E-step, calculate the probability of sample

$$\omega_l = p(\Upsilon^i = j \mid x^i; \Sigma_l, \Phi, \boldsymbol{\mu}, \boldsymbol{\Sigma}) \tag{21}$$

where Υ^i is a latent variable, represents the probability that the *i*th sample belongs to each Gaussian component.

M-step, update the model parameter

$$\begin{cases} \phi_j = \dfrac{1}{M}\sum_{i=1}^{M}\omega_j^i \\ \mu_j = \dfrac{\sum_{i=1}^{M}\omega_j^i x^i}{\sum_{i=1}^{M}\omega_j^i} \\ \Sigma_j = \dfrac{\sum_{i=1}^{M}\omega_j^i (x^i - \mu_j)\omega_j^i (x^i - \mu_j)^T}{\sum_{i=1}^{M}\omega_j^i} \end{cases} \tag{22}$$

Iterate over the Equation (21) and Equation (22), until the parameter converges to stable values.

3.3. Fusion

In VTL, the innovation covariance was extracted for GMM cluster analysis. We assign ω_k^E and ω_k^U to be the weights of EKF and UFIR, respectively. After we obtain the Gaussian weights of the samples according to the two steps above, the fusion weights in Figure 3 can be computed as:

$$W_k = \begin{bmatrix} \omega_k^E & \omega_k^U \end{bmatrix} \tag{21}$$

Furthermore, the JF estimate can be given as:

$$\hat{X}_k = W_k \left[\hat{X}_k^E \quad \hat{X}_k^U \right]^T = \omega_k^E \hat{X}_k^E + \omega_k^U \hat{X}_k^U \qquad (21)$$

where $\hat{X}_k^E$ and $\hat{X}_k^U$ are the estimates of EKF and UFIR, respectively.

4. Results and discussion

In this section, we 1) verified the effectiveness of designing VTL with UFIR filter, 2) evaluated the performance of the proposed method. To accomplish this objective, a vehicle-mounted experiment was carried out. The experimental data were processed using the EKF-, UFIR- and JF-based VTLs, and some comparative analyses of these three kinds of VTLs are also provided.

4.1. Experimental setup

Fig. 4 presents the experiment set up of the field test, trajectory and the sky plot of visible satellites. The experiment was implemented in an open area of Hong Kong. The experiment equipment includes the vehicle, NovAtel GPS antenna, NLS Stereo front-end, and laptop. Specifically, the raw satellite signals are first collected by the antenna that fixed to the top of the car, and then down convert to the intermediate frequency (IF) signal by the front-end. Finally, the data is saved in the computer for post-processing, in which an open-sourced GPS software-defined receiver (SDR) was used. The key parameter settings are listed in Table 1.

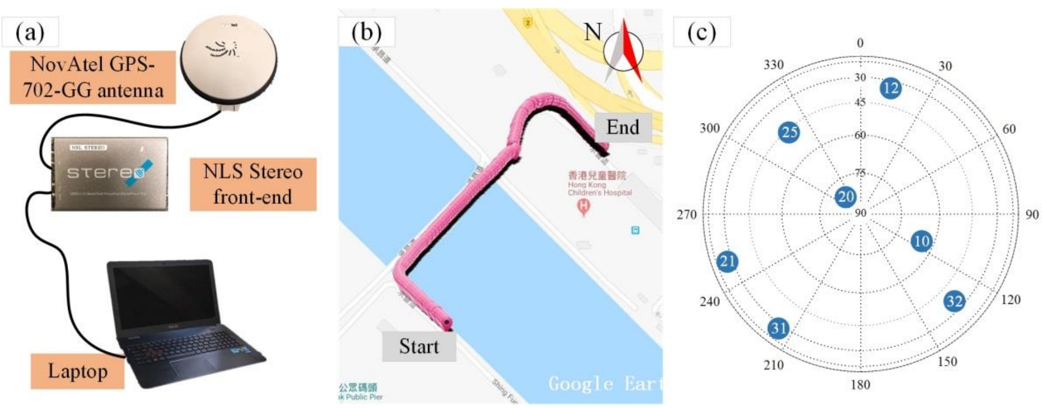

Fig. 4. Experiment setup and sky plot of visible satellites

Table 1
Parameters settings.

Parameter	Value	Unit
GNSS signal type	GPS L1 C/A	-
Intermediate frequency	6.5	MHz
Sampling rate	26	MHz
Coherent integration time	1	ms
VTL type	EKF/UFIR/JF	-

4.2. Results

A: Feasibility validation of UFIR-VTL

In Figure 4(c), there are seven satellites available. Here we select the PRN 10 with the highest carrier-to-noise ratio (CNR=48 dB-Hz) as the objective. Figure 5 and 6 shows the code phase and frequency error curves of PRN10, respectively, since the code phase errors and code frequency errors are important performance indexes in the VTL. The loop tracking time is 20 seconds. Because it is difficult to adjust the process and measurement noise statistics through the hardware devices, draw on some common knowledge, we assign undesired measurement noise covariance in the periods of 8-12 seconds to simulate noise interference. As we can see from Fig. 5 and 6, the UFIR-VTL can produce tracking accuracy that is slightly worse than EKF-VTL, where the statistics of noise is exactly known. However, under the noise interference in the periods of 8-12 seconds, the tracking results of EKF show a larger error than that of UFIR. The above analyses demonstrate that the EKF does not suit well the noise interference in VTL, while the UFIR is a better robustness way to against the noise uncertainties in the GNSS receiver. The root-mean-square errors (RMSEs) of two evaluation indexes are given in Table 2.

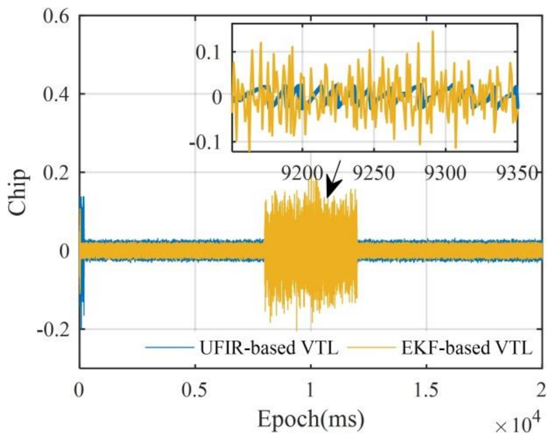

Fig. 5. Code phase errors of PRN 10.

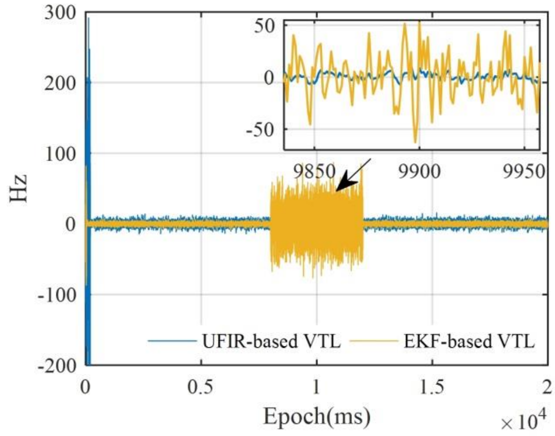

Fig. 6. Code frequency errors of PRN 10.

Table 2
RMSEs of code phase and frequency errors under different noise conditions.

Methods	RMSEs of code phase errors (Chip)		RMSEs of code frequency errors (Hz)	
	Without	With	Without	With
EKF-VTL	0.028	0.081	6.20	25.30
UFIR-VTL	0.030	0.031	6.40	6.47

B: Performance evaluation of JF

In this section, we mainly focus on accessing the performance of the JF algorithm. Since the fused information is the state vector in VTL, the horizontal and vertical positioning errors are used as evaluation indexes. To evaluate the positioning accuracy of the proposed JF method, we used the NovAtel Flexpak6, as a reference receiver to provide a benchmark trajectory. Fig. 7 shows the three-dimensional position RMSEs values of

EKF-, UFIE- and JF-methods. As can be seen, the accuracy of EKF is slightly better than that of UFIR under normal conditions. However, during the segment of noise interference, the EKF output shows a larger error than UFIR, which is an outcome of the ignorance of noise statistics. Furthermore, according to the subgraphs in Fig. 7, the JF can produce good positioning results of the whole process compare with the other two methods. Specifically, the proposed method can always close to the optimal filter regardless of the presence or absence of noise interference. This is owing to the probabilistic weights provided by the GMM cluster. Fig. 8 depicts the results of the probabilistic weight of EKF and UFIR, respectively. When the noise condition is ideal, the weights of EKF are relatively large, while in the case of noise interference, the weights of UFIR do. The results imply that the weights can be adjusted adaptively according to the noise conditions.

Thus, as shown in Fig. 9, the JF combines the optimality of EKF and the robustness of UFIR tends to achieve the most accurate estimation results overall.

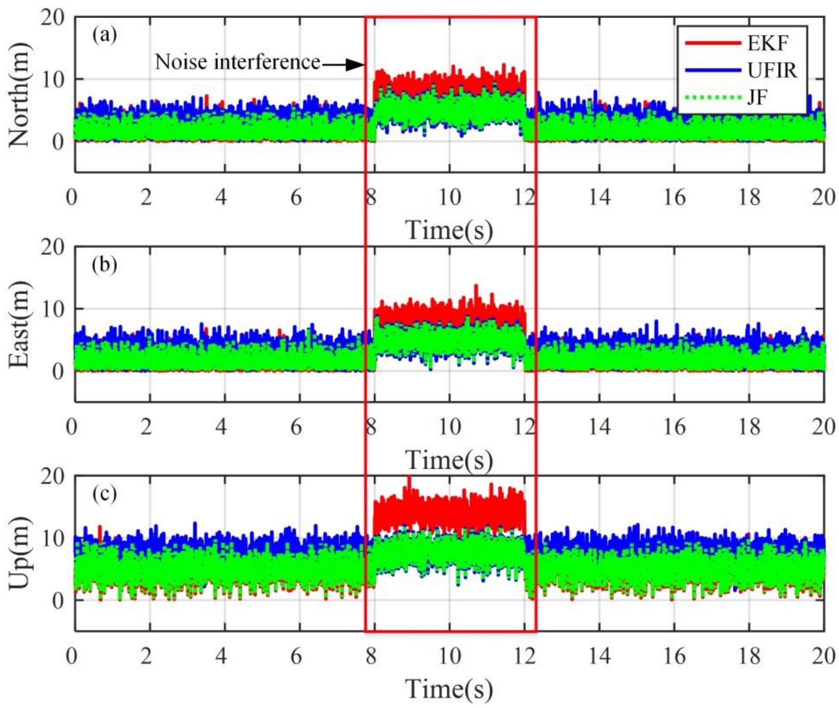

Fig. 7. Position RMSEs of EKF, UFIR, and JF, respectively. (a) North; (b) East; (c) Up.

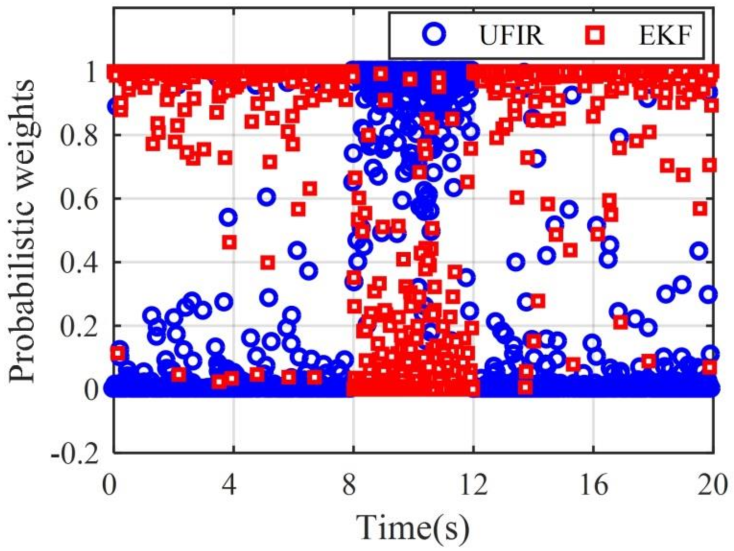

Fig. 8. The probabilistic weights of the EKF and UFIR, respectively.

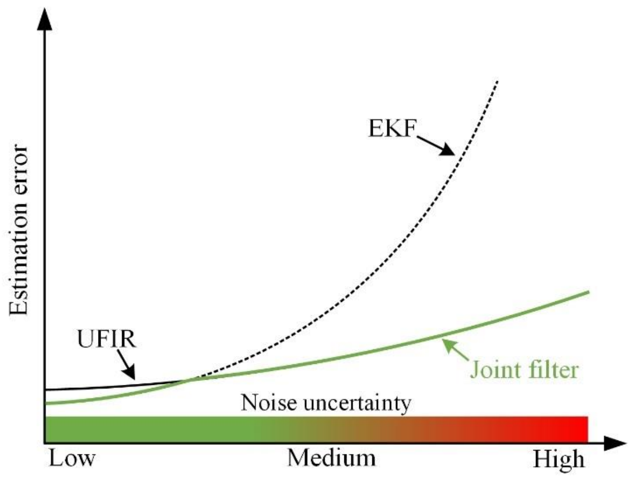

Fig. 9. Performance of EKF, UFIR and JF filters under different noisy environments.

5. Conclusion

The conventional EKF-based VTL is impractical, as it depends on the measurement noise statistics and is an uncertain process requiring manual experience. In this paper, a joint filter approach based on the EKF and UFIR algorithms is proposed, to enhance the VTL performance in GNSS-noisy environments. To achieve this, the UFIR was first applied to build VTL, which demonstrated more robust than EKF-based VTL but at the cost of a little precision while the noise interference occurred. To provide a better joint effect, the probabilistic weights of EKF and UFIR is determined using the GMM clustering algorithm. Moreover, the performance of the joint model is evaluated by a car-mounted experiment. The experiment results show that compare with the other two methods, the proposed JF can effectively ensure not only the optimal estimation but also the robustness. The fusion of the inertial navigation system (INS) and GNSS will be studied in our future work.

Author Contributions

J.D. and L.D. conceived and designed the simulation; B.X. assisted to collect the real GPS signal data and revise the paper; J.D. drafted the manuscript.

Declaration of competing Interest

The authors declare no conflict of interest.

Acknowledgments

The authors would like to thank the anonymous reviewers of their valuable comments. This work was partly supported by the National Natural Science Foundation of China (grant number 60904085), Foundation of National Key Laboratory of Transient Physics, and Foundation of Defence Technology Innovation Special Filed.

Reference

[1] C.C.R. Garcez, D.V. de Lima, R.K. Miranda, F. Mendonça, J.P.C.L. da Costa, A.L.F. de Almeida, R.T. de Sousa, Tensor-based subspace tracking for time-delay estimation in GNSS multi-antenna receivers, Sensors (Switzerland). 19 (2019) 1–15. https://doi.org/10.3390/s19235076.

[2] Z. Sun, X. Wang, S. Feng, H. Che, J. Zhang, Design of an adaptive GPS vector tracking loop with the detection and isolation of contaminated channels, GPS Solut. 21 (2017) 701–713. https://doi.org/10.1007/s10291-016-0558-5.

[3] H. Nourmohammadi, J. Keighobadi, Decentralized INS/GNSS System with MEMS-Grade Inertial Sensors Using QR-Factorized CKF, IEEE Sens. J. 17 (2017) 3278–3287. https://doi.org/10.1109/JSEN.2017.2693246.

[4] L.T. Hsu, Y. Gu, S. Kamijo, 3D building model-based pedestrian positioning method using GPS/GLONASS/QZSS and its reliability calculation, GPS Solut. 20 (2016) 413–428. https://doi.org/10.1007/s10291-015-0451-7.

[5] B. Xu, L.T. Hsu, Open-source MATLAB code for GPS vector tracking on a software-defined receiver, GPS Solut. 23 (2019) 1–9. https://doi.org/10.1007/s10291-019-0839-x.

[6] M. Lashley, D.M. Bevly, J.Y. Hung, Performance analysis of vector tracking algorithms for weak GPS signals in high dynamics, IEEE J. Sel. Top. Signal Process. 3 (2009) 661–673. https://doi.org/10.1109/JSTSP.2009.2023341.

[7] M. Lashley, D.M. Bevly, Comparison in the Performance of the Vector Delay / Frequency Lock Loop and Equivalent Scalar Tracking Loops in Dense Foliage and Urban Canyon, Proc. 24th Int. Tech. Meet. Satell. Div. Inst. Navig. (ION GNSS 2011), 20-23 Sept. 2011. (2011) 1786–1803.

[8] B. Xu, Q. Jia, L.-T. Hsu, Vector Tracking Loop-Based GNSS NLOS Detection and Correction: Algorithm Design and Performance Analysis, IEEE Trans. Instrum. Meas. PP (2019) 1–1. https://doi.org/10.1109/tim.2019.2950578.

[9] Q. Zhang, Y. Yang, Q. Xiang, Q. He, Z. Zhou, Y. Yao, Noise Adaptive Kalman Filter for Joint Polarization Tracking and Channel Equalization Using Cascaded Covariance

Matching, IEEE Photonics J. 10 (2018) 1–11. https://doi.org/10.1109/JPHOT.2018.2797050.

[10] S. Chen, Y. Gao, Improvement of carrier phase tracking in high dynamics conditions using an adaptive joint vector tracking architecture, GPS Solut. 23 (2019) 1–10. https://doi.org/10.1007/s10291-018-0806-y.

[11] H. Lin, Y. Huang, X. Tang, G. Sun, G. Ou, A robust vector tracking loop based on diagonal weighting matrix for navigation signal, Adv. Sp. Res. 60 (2017) 2607–2619. https://doi.org/10.1016/j.asr.2017.01.030.

[12] F. Jiancheng, Y. Sheng, Study on innovation adaptive EKF for in-flight alignment of airborne POS, IEEE Trans. Instrum. Meas. 60 (2011) 1378–1388. https://doi.org/10.1109/TIM.2010.2084710.

[13] Y.S. Shmaliy, A Kalman-like FIR estimator ignoring noise and initial conditions, Eur. Signal Process. Conf. 59 (2011) 985–989.

[14] J. Contreras-Gonzalez, O. Ibarra-Manzano, Y.S. Shmaliy, Clock state estimation with the Kalman-like UFIR algorithm via TIE measurement, Meas. J. Int. Meas. Confed. 46 (2013) 476–483. https://doi.org/10.1016/j.measurement.2012.08.003.

[15] S. Zhao, Y.S. Shmaliy, F. Liu, Fast Kalman-like optimal FIR filter for time-variant systems with improved robustness, ISA Trans. 80 (2018) 160–168. https://doi.org/10.1016/j.isatra.2018.07.012.

[16] S. Zhao, Y.S. Shmaliy, C.K. Ahn, F. Liu, Adaptive-Horizon Iterative UFIR Filtering Algorithm with Applications, IEEE Trans. Ind. Electron. 65 (2018) 6393–6402. https://doi.org/10.1109/TIE.2017.2784405.

[17] J. Zhao, G. Xie, D. Li, M. Song, Improved GMM-based method for target detection, IET Networks. 9 (2020) 7–11. https://doi.org/10.1049/iet-net.2019.0038.

[18] X. Zhang, X. Zou, M. Sun, T.F. Zheng, C. Jia, Y. Wang, Noise Robust Speaker Recognition Based on Adaptive Frame Weighting in GMM for i-Vector Extraction, IEEE Access. 7 (2019) 27874–27882. https://doi.org/10.1109/ACCESS.2019.2901812.